

Article

Evolution of Storm Surges over the Little Ice Age Indicated by Aeolian Sand Records on the Coast of the Beibu Gulf, China

Zhi Chen ^{1,2}, Baosheng Li ^{3,4}, Fengnian Wang ^{5,*}, Shuhuan Du ⁶, Dongfeng Niu ⁷, Yinjun Zhao ² and Yuejun Si ^{2,*}

¹ School of Geography and Planning, Sun Yat-sen University, Guangzhou 510275, China; chenzhi01111@nncu.edu.cn

² School of Geography and Planning, Nanning Normal University, Nanning 530001, China; yinjunzhao@nncu.edu.cn

³ State Key Laboratory of Loess and Quaternary Geology, Institute of Earth Environment, Chinese Academy of Sciences, Xi'an 710061, China; libsh@scnu.edu.cn

⁴ School of Geography, South China Normal University, Guangzhou 510631, China

⁵ School of Geography and Tourism, Huizhou University, Huizhou 516007, China

⁶ Key Laboratory of Ocean and Marginal Sea Geology, South China Sea Institute of Oceanology, Chinese Academy of Sciences, Guangzhou 510301, China; shuhuandu@scsio.ac.cn

⁷ School of Physics Science & Technology, Lingnan Normal University, Zhanjiang 524048, China; 250001@nncu.edu.cn

* Correspondence: wfn@hzu.edu.cn (F.W.); siyuejun@nncu.edu.cn (Y.S.)

Abstract: The Wutou section, hereinafter referred to as “WTS”, lies in Jiangping, Guangxi Province, China (21°32′8.25″ N, 108°06′59.9″ E; thickness of 246 cm) and consists of fluvial-lacustrine facies and dune sands of the Late Holocene. This study reconstructed the evolution of storm surges along the coast of the Beibu Gulf, Guangxi over the Little Ice Age, based on three accelerator mass spectrometry (AMS)-14C, optically stimulated luminescence (OSL) dating ages, and the analyses of grain size and heavy minerals. The analysis results indicated that the storm sediments interspersed among aeolian sands, lagoon facies, and weak soil display a coarse mean grain size and poor sorting. The storm sediments also show high maturity of heavy minerals and low stability resulting from rapid accumulation due to storm surges originating from the land-facing side of the coastal dunes. Records of seven peak storm surge periods were recorded in the WTS over the past millennium and mainly occurred after 1400 AD, i.e., during the Little Ice Age. The peaks in storm surges, including the 14Paleostrom deposit (hereinafter referred to as “Pd”) (1425–1470AD), 10Pd (1655–1690AD), 6Pd (1790–1820AD), and 4Pd (1850–1885AD) approximately corresponded with the periods of minimum sunspot activity, suggesting that the periods of storm surge peaks revealed by the WTS were probably regulated to a great extent by solar activity.

Keywords: coastal aeolian sands; Beibu Gulf in Guangxi; over the Little Ice Age; storm surge; grain size



Citation: Chen, Z.; Li, B.; Wang, F.; Du, S.; Niu, D.; Zhao, Y.; Si, Y.

Evolution of Storm Surges over the Little Ice Age Indicated by Aeolian Sand Records on the Coast of the Beibu Gulf, China. *Water* **2021**, *13*, 1941. <https://doi.org/10.3390/w13141941>

Academic Editor: Guobin Fu

Received: 10 June 2021

Accepted: 11 July 2021

Published: 14 July 2021

Publisher's Note: MDPI stays neutral with regard to jurisdictional claims in published maps and institutional affiliations.



Copyright: © 2021 by the authors. Licensee MDPI, Basel, Switzerland. This article is an open access article distributed under the terms and conditions of the Creative Commons Attribution (CC BY) license (<https://creativecommons.org/licenses/by/4.0/>).

1. Introduction

The waters north of the equatorial western Pacific Ocean experience the highest frequency of tropical cyclones globally. As one of the countries in the region most affected, China has experienced increasingly serious losses from abnormal typhoon activity in recent years [1]. Therefore, there is increased interest in approaches to mitigating damage from typhoons. The relatively short record of storms poses a challenge to analyzing the long-term evolution of storm events. Hence, alternative proxy records of long-term storm activity are required [2–15].

At a global level, coastal dunes positioned at the highest position of a storm wave or above the maximum astronomical tidal line [16,17] are widely developed in coastal zones with abundant sand sources and strong shoreward winds. Periodicity is evident in the evolution of these dunes and their sedimentary characteristics and distribution can act as a

long-term historical record of sea level fluctuations and changes to the paleogeographic environment [18,19]. Consequently, studies on these dunes have taken on increasing importance in global change research. Studies on the development of coastal dunes have attracted increasing attention over the last few decades as historical records of typhoon activity [20–27]. The increased severity of storm surges resulting from strong typhoons can erode and transport materials from coastal hills to lowlands [28], resulting in abrupt changes in the grain sequence and structure of landside deposits. Therefore, the study of coastal dunes can allow the retroactive deduction of historical typhoon storm surge activity [29–32].

The sand dune activity along the south coast of China since the late Holocene has resulted in a discontinuous distribution of sand dunes in the coastal area of Fujian-Guangxi [19]. The coastal zone sedimentary system formed by the sand bar-lagoon and overlying sand along the coast of Jiangping Town, Fangchenggang City, Guangxi Province is ideal for studying the formation and evolution of coastal dunes with the purpose of reconstructing ancient storm surge activities. The present study selected a 246 cm coastal dune profile in the southern part of Wutou. A chronological framework was established to reconstruct the history of coastal storm surge activity during the late Holocene in this area according to grain size and the indicative significance of heavy minerals to the environment.

2. Study Area

The Guangxi coastal zone lies southwest of the South China uplift zone and has experienced a gradual rising process since the postglacial period [33]. The coastal sand bar-lagoon system accounts for ~20% of the total shoreline length of Guangxi Province, second only to that in Shandong Province [34]. Jiangping Town lies at the southwest end of this coastal zone and southeast of Dongxing (21°35′22″ N, 108°07′44″ E) (Figure 1). The exposed bedrock in this area mainly consists of sandstone and siltstone of the Silurian period during the Lower Paleozoic and Jurassic periods of the Mesozoic era [35], as well as overlying loose sediments of the late Quaternary Jiangping (Q_j) and Guiping formations (Q_g), floodplain facies, marine facies, coastal plain facies, and coastal dune facies [36]. The elevation of the area decreases from northwest to southeast and can be divided into three geomorphic blocks distributed roughly parallel to the shoreline: (1) the platform, (2) the lagoon, and (3) the sand bar. Since the middle and late Holocene, the sand bar-lagoon has been mostly covered with grass and shrub dunes with a height of 2 m [18]. Jiangping Town has a tropical marine monsoon climate with an average annual temperature and rainfall of 24.5 °C and >1500 mm, respectively, with the rainy season occurring mainly from July to September. The prevailing wind directions of the study area are northeast. The mean tidal range is 2.12 m. The tortuous shoreline of the study area results in typhoon storm surges forming in the crests of many bays at heights exceeding the average height by 2 m [37].

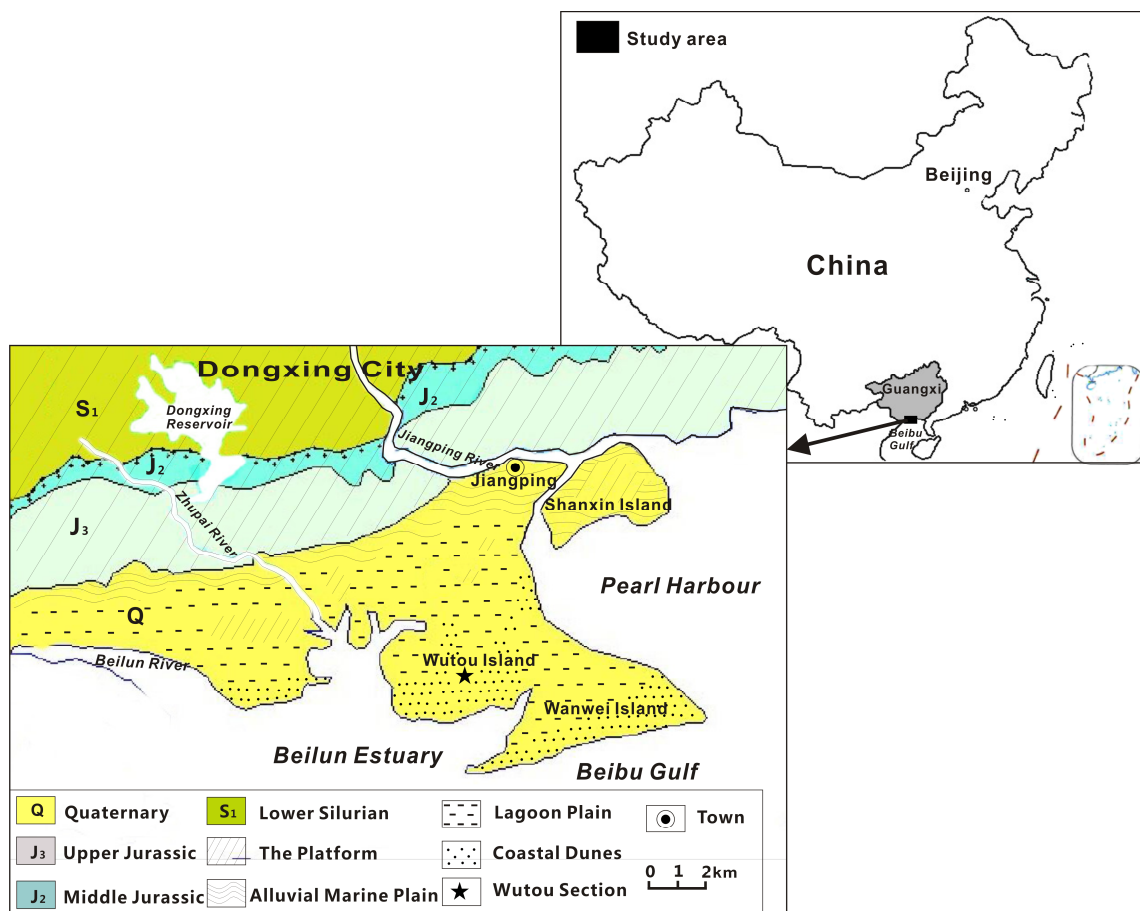


Figure 1. Stratigraphic map of the Wutou section.

3. Sequence of Aeolian Sand and the Age of the Wutou Section in Jiangping

3.1. Wutou Section

The Wutou section, hereinafter referred to as “WTS”, lies in the interdune land of the transverse sand ridges southwest of Wutou Village, Jiangping Town (21°32′8.25″ N, 108°06′59.9″ E). The WTS lies ~800 m to the south of the coastline (Figure 1) and consists of gentle undulating shrub dune land. The profile of the WTS has a thickness of 246 cm and from top to bottom is classified into seven layers of moving dune (hereinafter referred to as “D”) and seven layers of storm deposits (Pd) by color, structure, and the overlying–underlying contact modes of the layers. The mobile dune is light-yellow, mainly consists of medium-fine sands and has horizontal bedding and cross bedding. The storm deposits comprise mainly loose, carbon-bearing offwhite-caesious medium-fine sands with a horizontal texture and flat bottom surface. The interspersed aeolian sand and storm deposits form distinct rhythmic deposits. The WTS integrated contact with gray-black lake-marsh facies at the bottom.

3.2. Chronological Result

One optically stimulated luminescence (OSL) and two AMS-¹⁴C dating samples were collected from the top and bottom of the WTS. The samples were analyzed and tested at the Miami Beta Labs, United States of America (USA) and the Neotectonic Geochronology Laboratory, Institute of Geology, China Earthquake Administration, respectively. The OSL samples were dated using single-aliquot regenerative-dose (SAR) (Risø TL/OSL-DA-20 Thermoluminescence/OSL Instrument, Risø Lab, Denmark) for the extraction of coarse quartz particles of 90–125 μm. AMS-¹⁴C was used to determine the contents of organic matter and carbon debris in the strata of the material system. The obtained conventional

ages were corrected by fractionation and then by IntCal 13 data [38] to obtain estimates of the calendar age. As shown in Table 1 and Figure 2, the lacustrine facies disappeared and coastal aeolian sand accumulated in the WTS at 530a BP, around 1400 AD, corresponding to the beginning of the Little Ice Age, hereinafter referred to as “LIA”. The study area demonstrates a stable rising process and source supply since the postglacial period [33]. The prevailing wind direction of the coastal region of South China is northeast and hasn’t changed much since the middle-late Holocene [19]. Therefore, the aeolian sands of WTS have the same occurrence and color and show a continuous accumulation apart from occasional storm surge deposits.

Table 1. Results of optically stimulated luminescence (OSL) and accelerator mass spectrometry (AMS)- ^{14}C dating for the Wutou section.

Sample	Depth (cm)	Age (a BP)	Calendar Age (cal. A.D.)
WTS4-M	34	120 ± 30 (AMS- ^{14}C age)	1940~1880
OSL-7-B	82	20 ± 40 (OSL age)	—
WTS15-T	250	500 ± 30 (AMS- ^{14}C age)	1448~1398

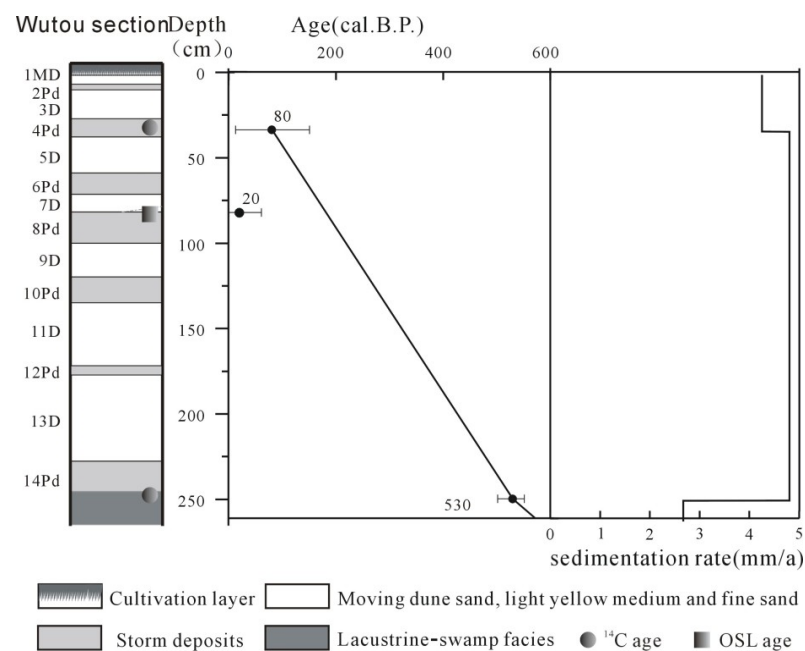


Figure 2. Age and sedimentation rate of the Wutou section.

There was obvious inversion of the OSL age of 20 ± 40 a BP at 82 cm depth, possibly due to disturbance and pollution; therefore, the present study disregarded this record. The plant root system may be an occasional disturbance to the OSL age of the 7D layer and can’t be ruled out [39]. But for the AMS- ^{14}C age of the 4Pd layer, there are large carbonaceous fragments reserved in situ, so the disturbance is less likely. In addition, the area and the scale of the coastal sands are in continuous decline [40]; however, the OSL age-dating result does not correspond with this situation. For the WTS, it is reliable to define the accumulation time from beginning to end with the AMS- ^{14}C age dating from the carbonaceous fragments sample reserved in the 4Pd layer and the organic material sample reserved in the 15LS layer.

The sedimentation rate of this section was calculated based on the results of two age tests at the top and bottom of the section. Linear interpolation of the age was performed and the chronology framework of sedimentation of WTS was established (Figure 2). As

shown in Figure 2, the sedimentation rate of the coastal aeolian sand profile was relatively stable, ranging from 4.25 mm a^{-1} to 4.8 mm a^{-1} .

4. Analyses of Particle Sizes and Heavy Minerals of the WTS

4.1. Particle Size Analysis

Samples ($n = 132$) were collected from the WTS at a depth interval of 2 cm. Grain-size analysis was conducted at the Key Laboratory of Environmental Evolution and Resource Utilization of Beibu Gulf, Ministry of Education, Nanning Normal University using a Malvern Mastersizer 2000 M laser particle size analyzer with a measuring range of 0.01–2,000 μm . The experimental process used was based on the loess particle size analysis method [41].

As shown in Table 2, the sand content of WTS samples exceeded 90%, with fine sand comprising the largest proportion, followed by medium sand. The aeolian sand layer of the WTS samples was the same as that of modern coastal aeolian sand in the surrounding area [42] and was mostly composed of sand without silt clay. The content of fine sand in the aeolian layer was the highest among the entire profile. The contents of medium and coarse sand in the storm deposit layer were the highest across the entire section. Very coarse sand was found in some samples, whereas there were decreases in the contents of fine sand, very fine sand, silt, and clay.

Table 2. Grain-size composition (%) of different sedimentary facies and main descriptive statistics (expressed in Φ units) in Wutou section and other sites.

Site	Facies		Coarse Sand	Medium Sand	Fine Sand	Very Fine Sand	Coarse Silt	Fine Silt	Clay	Mz(Φ)	$\sigma(\Phi)$
WTS	whole section 183		0–5.39	20.40–50.19	46.07–79.11	0.02–1.47	0–2.78	0–1.06	0–1.06	1.94–2.35	0.41–0.62
		average	0.40	36.43	62.77	0.31	0.06	0.02	0.02	2.16	0.48
	aeolian sand layer 92		0–1.36	20.40–46.55	52.05–79.11	0.02–1.47	0	0	0	2.03–2.35	0.41–0.55
		average	0.15	33.28	66.21	0.36	0	0	0	2.22	0.46
	storm deposits layer		0.03–5.39	34.21–50.19	46.07–63.91	0.02–1.27	0–2.78	0–1.06	0–1.057	1.94–2.22	0.45–0.62
		average	0.80	41.41	57.32	0.25	0.15	0.04	0.04	2.10	0.51
Jianling in Hainan Island [10]	aeolian sand layer		23.49	52.36	24.15			0		1.50	0.68
	storm deposits layer		39.35	42.72	17.16			0.77		1.22	0.83
Zhoushan Island in Zhejiang(sand dune) [23]	Before typhoon									2.20	0.37
	After typhoon									1.97	0.45
Hatteras Island in southeastern America (sand dune) [43]	Before typhoon									1.98	1.37
	After typhoon									1.74	1.54

The present study calculated the average particle size $Mz(\phi)$ and sorting coefficient $\sigma(\phi)$ of the WTS according to the formula proposed by Folk and Ward [44]. As shown in Figure 3, the results indicated that the sediments in the WTS can be characterized as medium-fine sand and the range of sorting of sediments in the section was good to poor. Among the sediment particles, storm deposits had the coarsest grain size, followed by aeolian sand and lagoonal facies, with weak sandy loam showing the finest grain size. The value of $\sigma(\phi)$ confirmed optimal sorting in the aeolian sand, followed by that in the storm deposits and weak sandy loam. Lagoonal facies showed the worst sorting, with a relatively high content of fine particulate matter, such as clay (Table 2). These differences in $\sigma(\phi)$ resulted in the grain size parameters displaying a vertical rhythm of peak–valley alternation (Figure 3).

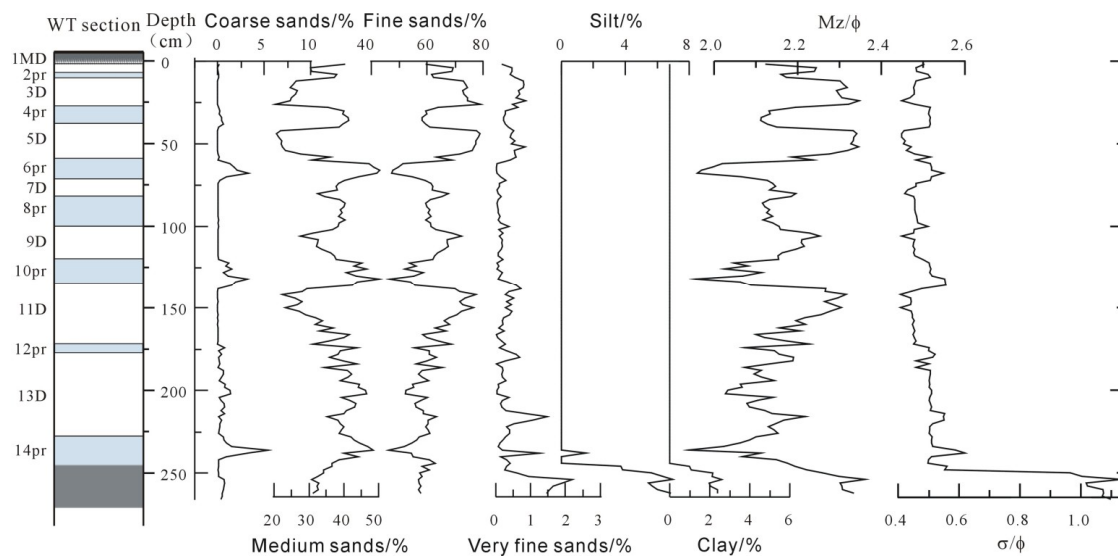


Figure 3. The percentage and parameters of grain-size distributions in the Wutou section.

4.2. Analysis of Heavy Minerals

Heavy mineral analysis was performed on 14 samples and 2 samples from the WTS and modern beach sands, respectively. The heavy minerals content of these samples fluctuated between 0.14% and 1.40%, with 22 common species. Among the minerals identified, ilmenite, white titanium, tourmaline, and zircon showed the highest concentrations, collectively accounting for 88.62% of all heavy minerals. These minerals are dominant in the WTS and the sediments of nearby rivers [45], beaches, and shallow seas [46] (Table 3). Hematite, anatase, and rutile collectively accounted for 5.72% of all heavy minerals. Only minor concentrations of epidote, monazite, garnet, amphibole, pyroxene, chrome spinel, pyrite, malachite, and sillimanite were detected, collectively contributing less than 1% of all minerals. The heavy mineral component also contained 1.47–5.51% of debris and weathered minerals. The average content of heavy minerals in the storm deposit layer was 0.63%, exceeding that of the aeolian sand layer of 0.60%.

Table 3. Heavy mineral composition (%) in different sedimentary facies of the Wutou section.

Site		Ilmenite	White Titanium	Zircon	Tourmaline	Hematite	Anatase	Rutile	Epidote	Monazite	Others
WTS	D	17.21–50.40	13.27–31.71	4.71–12.91	5.43–17.85	0.40–4.48	0.93–4.79	1.19–2.58	0.17–3.45	0.169–0.172	2.33–4.61
	average	42.44	23.53	9.63	10.48	1.61	2.10	1.83	1.00	0.17	3.64
WTS	Pd	33.83–59.72	10.53–38.76	5.22–13.82	6.51–14.72	0.26–6.78	0.41–3.07	0.86–2.35	0.18–0.78	0.16–0.17	1.47–5.51
	average	46.99	22.50	9.96	10.78	2.56	1.78	1.84	0.44	0.168	3.25
Gold beach	average	28.05–29.03	33.63–39.30	9.40–9.60	5.75–7.47	1.00–1.70	7.55–8.10	2.30–2.70	0.83–1.50		1.75–5.17
		28.54	36.47	9.50	6.61	1.35	7.83	2.5	1.17		3.46
Beibu Gulf [45,46]	average	55.80		23.10	38.70			10.80			
		56.00	12.20	9.5	10.60	4.30	4.15	0.60	1.70	1.20	
Fangcheng River [45,46]	average	75.40		49.80	4.30			2.60	3.00		
		50.00	6.00	7.00	6.00	18.00					

5. Discussion

5.1. Storm Surge Events Indicated by Storm Deposits in the WTS

The erosive actions of wind and waves during modern storm surges can lead to differences in grain size characteristics in different parts of a dune surface, depending on the surrounding topography, vegetation, and other comprehensive factors. The coarse grain size and poor sorting characteristics of storm deposits in the WTS are similar to that of coastal dunes in North Carolina [43], in Hainan [10], and Zhoushan [23] in Zhejiang Province after the effects of storms (Table 2). This observation suggests that storm deposition in this area is the product of backshore accumulation at the end of a storm surge. Storm deposits are characterized by a loose and “honeycombed” structure. This structure occurs

through rushing water generated by a storm depositing wet sands on top of previously dry sand dunes. The subsequent rapid draining of water generates this honeycombed and loose sand structure [47,48].

Sample points of each sedimentary facies in the WTS were projected onto the Passega C-M map according to particle size, with a median particle size corresponding to the 1% particle content. Within a C-M map, “C” represents the coarsest 1 percentile of sediment particles as an indicator of the upper limit of competence of a depositional agent, provided that a full range of sizes was available for particle transport; “M” represents the median 50th percentile of grain size, which reflects the average energy of ambient agents. C-M patterns not only reflect the transport and depositional mechanisms of sediments as a whole, but also indicate the flow path of coarse components. Therefore, this method has been widely used to reconstruct modern and ancient depositional environments. The sample points were mainly distributed in the QR section of the progressive suspension zone, there was a proportional increase in C and M, mostly parallel to the baseline of $C = M$, and the groups of sample points were significantly differentiated (Figure 4). The sample points of the storm deposit were located far from the $C = M$ baseline and had poor sorting. The C and M values of the samples all exceeded $400 \mu\text{m}$ and $200 \mu\text{m}$, respectively. The samples could be roughly separated from the aeolian sand samples by considering $M = 230 \mu\text{m}$ to be the boundary. The separated samples fell into the IV region, indicating high turbulence and that the sediment particles were mainly regulated by a transport medium characterized by stronger mobility and energy.

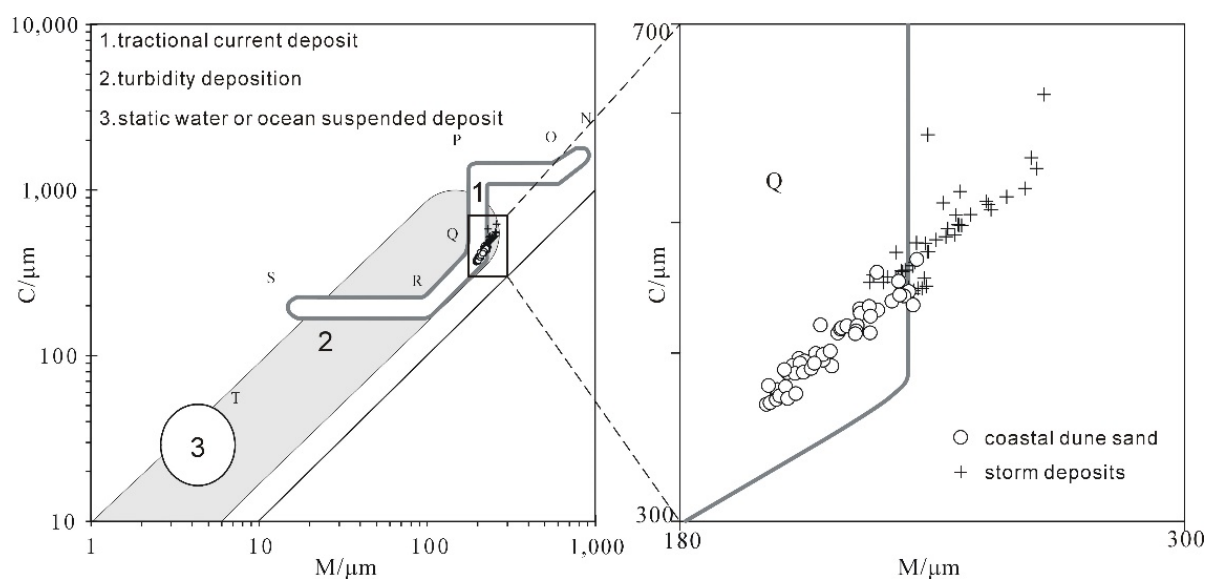


Figure 4. C-M schema of different facies in the Wutou section.

In addition to grain size, there were also differences in the stability coefficients of heavy minerals and in the ZTR index (Zircon-Tourmaline-Rutile maturity index) of storm deposits and aeolian sands. The mineral stability coefficient reflecting weather resistance represents the relative proportions of stable and unstable minerals [49]. The current study regarded the stability coefficient to be the ratio of extremely stable minerals to unstable minerals + relatively stable minerals + stable minerals. The ZTR index, or heavy mineral maturity index, is a method of determining how weathered a sediment is, and it represents the proportion of zircon, tourmaline, and rutile in total detrital heavy minerals [50]. Both the stability coefficient and the ZTR can reflect the distance of sediment transport and the levels of mechanical kinetic energy, hydrodynamic separation, abrasion, and maturity. The stability values of the storm deposit, aeolian sand, and modern beach sand at Jintan were 1.04, 1.36, and 1.41, respectively, whereas the ZTR values were 22.59, 21.94, and

18.61, respectively. The low maturity and high stability of modern beach sand in Jintan reflect the characteristics of an intertidal sedimentary environment. In other words, a low mechanical kinetic energy, long-term winnowing by sea water, and high dissolution strength. The aeolian sand that developed above the high tide line of the backshore was formed in a dry and windy environment in which heavier minerals in the beach sand could not be blown and transported to the backshore. Therefore, the minerals in the aeolian sand layer generally showed a low specific gravity. Storm deposits occur in relatively high-energy environments, characterized by high maturity and low stability of heavy minerals. This phenomenon fully demonstrates the action of high-energy force conditions dominated by mechanical action, indicating that the development of this type of sediment is triggered by an extreme event from a long distance away and that the sediment was rapidly transported ashore.

The accumulation triggered by tsunami extreme events shares characteristics with storm surge sediment in coastal areas, and there exist many disputes on technical distinction between sandy tsunami and storm deposits [43]. According to a numerical simulation, tsunami waves generated by a virtual extreme earthquake in the Manila Trench can cause severe hazards on the south coast of China, with a maximum wave amplitude over 8 m and velocity exceeding 2 ms^{-1} when it reaches the shore [51]. Simulation studies also show that the tsunami which destroyed the Song dynasty on Nan'ao island of Guangdong province in 1076 AD can reach the coastal region in mid-east Vietnam, but the Beibu Gulf area was only slightly affected by this tsunami due to a natural barrier of Hainan island [52]. No tsunami has ever been documented in the Beibu Gulf area since 1400 AD [53]. Therefore, taking the storm surge as a critical factor for the formation of aeolian sand over the LIA is reliable. The formation of coastal storm surge sediments in the Beibu Gulf is affected by high energy forces and the characteristics of rapid and long-distance sediment transport can be established by low and high $Mz(\phi)$ and $\sigma(\phi)$ values, respectively, high maturity, and low stability of heavy minerals. Therefore, the parallel cycles of change in $Mz(\phi)$ and $\sigma(\phi)$ in the seven storm deposition layers in the WTS can be regarded as seven periods of typhoon storm surges under a background of coastal aeolian sand accumulation. If this view is correct, the WTS has recorded at least seven periods of high storm surges since 1400 AD.

5.2. Evolution of the Coastal Environmental in the Beibu Gulf since the Late Holocene and the Significance of High-Energy Sea-Atmosphere Events

Simulation studies have shown that the northern part of the South China Sea experiences a similar water-increasing effect before and after a typhoon [54]. Therefore, it can be concluded that the period of high storm surges during the LIA as revealed by the grain size and heavy mineral content of the WTS was universal across the South China Sea. Current study suggests that the peak in storm surge events since the LIA in the coastal areas of South China was concentrated during 1500 AD and 1660–1680 AD. For example, historical data for Guangdong Province indicates an increase in the number of typhoons that have landed over the past millennium since 1460 [7] and that typhoons impacted Guangdong during the 17th and 19th centuries [12,13]. Sedimentary records for Guangjin Island in Xisha, South China Sea [7] and for Lingshui, Hainan [10] similarly confirmed that the maximum typhoon frequency occurred in the northern part of the South China Sea since 1400 AD, particularly during 1600–1900 AD [13].

The WTS shows records of seven periods of high storm surges in the Beibu Gulf since the LIA: (1) 1420–1470 AD (14Pd), (2) 1520–1610 AD (12Pd), (3) 1650–1690 AD (10Pd), (4) 1730–1770 AD (8Pd), (5) 1790–1800 AD (6Pd), (6) 1850–1890 AD (4Pd), and (7) 1930–1940 AD (2Pd). The earliest historical description of typhoons and associated disasters in the Beibu Gulf can be traced back to 972 AD. Descriptions of the typhoon or associated disasters were identified in the data, with keywords searched to identify the former being “wind disaster”, “strong wind”, and “hurricane”, whereas those for the latter included “sea overflow”, “great wind and rain”, and “wind tide”. For example, both the Wuxing annal/Lingshan annal of the Ming Dynasty and the Lingshan annals of the Republic of

China (Qing Dynasty, Jiaqiāng) recorded a rise in sea water level in Lianzhou and Lingshan in 1501. Historical records for May of 1653 stated: “In May, the sea overflowed in Qinzhou” and “On the 4th of May, Lianzhou was hit by a hurricane and the sea tide was overflowing” (Qing Dynasty, disaster annals/Hepuxian annal, Lianzhou annal); for June of 1802: “in June, Qinzhou Sea Overflow” (Qinzhou annals); in 1908, “Hepu hurricane occurred on 12 September and on 17 September, and the tide rose”; in 1934, “On the night of 18 June, a strong east wind came up in Qinxian, the sea water overflowed, the water was deep in Qingcaoping, Shapo and other places”. These historical records assisted in reconstructing the historical frequency of typhoons and storm surge disasters in the Beibu Gulf since the LIA was restored [55] (Figure 5b). The historical records indicated that the frequency of storm surge disasters gradually increased after 1500 AD. These disasters included the four “sea overflow” events in 1501, 1653, 1802, and 1934 (the black arrow in Figure 5b) which were basically within the range of the peak period of storm surges recorded in the WTS and are generally consistent with the conclusions of various studies in South China [8,13,56] and of islands within the South China Sea [7,10,12].

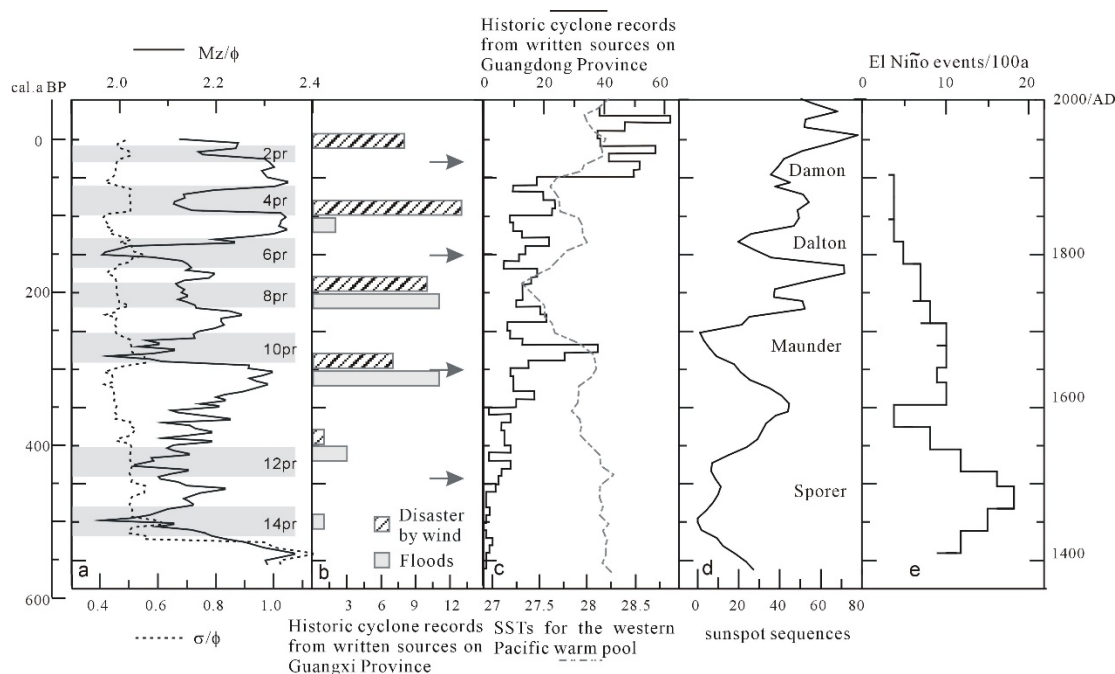


Figure 5. A comparison of the large tropical cyclone event periods in Beibu Gulf, Guangxi Province, China with paleo-cyclone records for the South China Sea over the LIA. (a) Large tropical cyclone event periods at the Wutou section (WTS) Scheme 55. (b) Historic cyclone records for Guangxi Province from written sources [51]. (c) Historic cyclone records for Guangdong Province from written sources [13]. Sea surface temperatures (SSTs) for the western Pacific warm pool (WPWP) from core MD98-2181 [57]. (d) Inferred changes in Holocene El Niño frequency from Laguna Pallcacocha, Ecuador [58]. (e) Sunspot sequences [59].

It is generally considered that the trends in climate change over the past millennium can be divided into three major periods: (1) the medieval warm period (MWP), (2) the LIA and, (3) the modern warm period. The sea surface temperatures (SST) in the Indian Ocean and in the Western Pacific Ocean were relatively high during the medieval warm period [57], and the sea level in the northern South China Sea was at least 128 cm higher than that today [60]. A high sea level event occurred in the estuary of the Pearl River [61,62] following which the sea level began to decline during the LIA. The records within the WTS indicated that lacustrine sediments dominated prior to 1400 AD, following which aeolian sediments representing cold and dry environments in the LIA dominated during (1400–2000 AD). These high storm surge periods, including 14Pd (1425–1470 AD), 10Pd (1655–1690 AD), 6Pd (1790–1820 AD), and 4Pd (1850–1885 AD), correspond with the

minimum phases of the Spörer, Maunder, Dalton, and Damon spots in the sunspot activity curve (Usoskin, et al., 2007), respectively, with sunspot activity and storm surge periods showing near synchronized changes. Although the relationship between solar activity and typhoon activity has yet to be isolated, solar activity has been linked to significant regional differences in global warming. Subtropical oceans with less cloud enhance meridional Hadley circulation after absorbing solar radiation [63]. The superposition of this positive feedback process will eventually adjust the entire low-latitude air-sea coupling system, thus affecting the air-sea cycle, leading to the active landing period of typhoons mostly occurring during the cold wave stage of the LIA [15]. Undoubtedly, the relationship between typhoon storm surge activity and solar activity on a millennium scale may not be so simple. Therefore, more detailed work on interpreting geological records for different climatic regions is required. In addition, there is a need for a discussion on chronology, resolution, significance of proxy indicators, and climate simulation, with a view to identifying mechanisms of climate change and storm surge activity over the LIA.

6. Conclusions

The WTS in the southwest of China's coastline has a thickness of 264 cm of aeolian sediments within which seven layers of storm deposits (Pd) can provide a medium for the study of paleo-storms. We reconstructed the evolution of coastal storm surges since the LIA in the Beibu Gulf coastal area according to grain size and the indicative significance of heavy minerals. These results suggest that (1) the mean grain size $Mz(\phi)$ and sorting coefficient σ were negatively correlated and showed a synchronous distribution in comparison to aeolian sand in the WTS. The high maturity and low stability of heavy minerals indicated that they are affected by high-energy forces and that they are the products of the rapid accumulation of sand dunes on the landward side of the coast subject to the influence of storm surges; (2) seven periods of high storm surges were recorded in the aeolian sand of the WTS since 1400 AD. Four of these periods correspond to minimum stages of sunspot activity. This correlation indicates that solar activity may to some extent affect the peak period of storm surges.

The results of the present study can provide novel perspectives and methods for the study of paleo-storms; however, this is only a starting point, and more research on the evolution mechanism of the paleo-storms in the Beibu Gulf coastal area would be worthwhile.

Author Contributions: Conceptualization, B.L. and Y.S.; methodology, Z.C. and Y.S.; software, Z.C.; validation, F.W. and S.D.; formal analysis, Z.C. and Y.S.; investigation, Z.C., D.N. and Y.S.; resources, S.D.; data curation, B.L.; writing—original draft preparation, Z.C.; supervision, B.L.; project administration, Y.S.; funding acquisition, F.W., Y.S. and Y.Z. All authors have read and agreed to the published version of the manuscript.

Funding: This research was funded by the Natural Science Foundation of Guangxi Province, China (grant number 2017GXNSFBA198126), Ph D research startup foundation of Nanning Normal University (grant number 0819-2014L08), Guangxi Scientific Project, China (grant number AD19110140), Guangdong Basic and Applied Basic Research Foundation (grant number 2020A1515011071) and Guangdong Innovation Project (grant number 2018KTSCX213).

Conflicts of Interest: The authors declare no conflict of interest.

References

1. Ying, M.; Zhang, W.; Yu, H.; Lu, X.; Feng, J.; Fan, Y.; Zhu, Y.; Chen, D. An overview of the China Meteorological Administration tropical cyclone database. *J. Atmos. Ocean. Technol.* **2014**, *31*, 287–301. [[CrossRef](#)]
2. Emanuel, K. Increasing destructiveness of tropical cyclones over the past 30 years. *Nature* **2005**, *436*, 686–688. [[CrossRef](#)] [[PubMed](#)]
3. Chan JC, L. Comment on Changes in tropical cyclone number, duration and intensity in a warming environment. *Science* **2006**, *311*, 1713. [[CrossRef](#)]
4. Huang, G.; Yan, W. Holocene storm deposits information of the Pearl Estuary indicated by foraminifera. *Chin. Sci. Bull.* **1997**, *42*, 423–426.

5. Xiong, H.; Zong, Y.; Huang, G.; Fu, S. Seabed erosion and deposition related to the typhoon activity of the past millennium on the southeast coast of China. *Earth Surf. Process. Landf.* **2020**, *45*, 1695–1704. [[CrossRef](#)]
6. Yu, K.F.; Zhao, J.X.; Collerson, K.D.; Shi, Q.; Chen, T.G.; Wang, P.X.; Liu, T.S. Storm cycles in the last millennium recorded in Yongshu Reef, southern South China Sea. *Palaeoecology* **2004**, *210*, 89–100. [[CrossRef](#)]
7. Chen, T.; Roff, G.; Feng, Y.; Zhao, J. Tropical Sand Cays as Natural Paleocyclone Archives. *Geophys. Res. Lett.* **2019**, *46*, 9796–9803. [[CrossRef](#)]
8. Chen, H.F.; Wen, S.Y.; Song, S.R.; Yang, T.N.; Lee, T.Q.; Lin, S.F.; Hsu, S.C.; Wei, K.Y.; Chang, P.Y.; Yu, P.S. Strengthening of paleo-typhoon and autumn rainfall in Taiwan corresponding to the Southern Oscillation at Late Holocene. *J. Quat. Sci.* **2012**, *27*, 964–972. [[CrossRef](#)]
9. Wang, L.C.; Behling, H.; Lee, T.Q.; Li, H.C.; Huh, C.A.; Shiau, L.J.; Chang, Y.P. Late Holocene environmental reconstructions and their implications on flood events, typhoon, and agricultural activities in NE Taiwan. *Clim. Past* **2014**, *10*, 1857–1869. [[CrossRef](#)]
10. Zhou, L.; Gao, S.; Jia, J.; Zhang, Y.; Yang, Y.; Mao, L.; Fang, X.; Shulmeister, J. Extracting historic cyclone data from coastal dune deposits in eastern Hainan Island, China. *Sediment. Geol.* **2019**, *392*, 105524. [[CrossRef](#)]
11. Li, H.C.; Zhao, M.; Tsai, C.H.; Mii, H.S.; Chang, Q.; Lee, K.Y. The first high-resolution stalagmite record from Taiwan: Climate and environmental changes during the past 1300 years. *J. Asian Earth Sci.* **2015**, *114*, 574–587. [[CrossRef](#)]
12. Chan, J.C.L.; Shi, J.E. Frequency of typhoon landfall over Guangdong Province of China during the period 1470–1931. *Int. J. Climatol.* **2000**, *20*, 183–190. [[CrossRef](#)]
13. Liu, K.B.; Shen, C.M.; Louie, K.S. A 1000-year History of Typhoon Landfalls in Guangdong, Southern China, Reconstructed from Chinese Historical Documentary Records. *Ann. Assoc. Am. Geogr.* **2001**, *91*, 453–464. [[CrossRef](#)]
14. IPCC. *Climate Change 2007, The Physical Science Basis. Contribution of Working Group I to the Fourth Assessment Report of the Intergovernmental Panel on Climate Change*; Cambridge University Press: Cambridge, UK, 2007.
15. Liu, K.; Fan, D. Global warming is causing the typhoon enhancements: Paleotempestology progress and implications. *Chin. Sci. Bull.* **2008**, *53*, 1489–1502.
16. Short, A.D.; Hesp, P.A. Wave, beach and dune interactions in southeastern Australia. *Mar. Geol.* **1982**, *48*, 259–284. [[CrossRef](#)]
17. Pye, K. Coastal dunes. *Prog. Phys. Geogr.* **1983**, *7*, 531–557. [[CrossRef](#)]
18. Huang, Z. Comparison of the paleodune formed during the late pleistocene between China and Japan. *Trop. Geogr.* **1993**, *13*, 1–12.
19. Wu, Z.; Huang, S.; Hu, S. *Research on the Landforms of the Wind-Drift Sand in South China Coast*; Science Press: Beijing, China, 1995; pp. 53–56.
20. Van de Graaff, J. Dune erosion during a storm surge. *Coast. Eng.* **1977**, *1*, 99–134. [[CrossRef](#)]
21. Vellinga, J. Beach and dune erosion during storms. *Coast. Eng.* **1982**, *6*, 361–387. [[CrossRef](#)]
22. Hesp, P.A. Surf zone, beach and foredune interactions on the Australian south east coast. *J. Coast. Res.* **1988**, *3*, 15–25.
23. Zhang, G.D.; Wang, Y.Y.; Zhu, J.C.; Yan, J.P. Modern coastal storm deposits of Putuo Island and Zhujiajiao Island, Zhoushan. *Acta Sedimentol. Sin.* **1987**, *5*, 17–28.
24. Dong, Y.; Namikas, S.L.; Hesp, P.A.; Ma, J. Field measurements of influence of sand transport rate on structure of wind-sand flow over coastal transverse ridge. *Chin. Geogr. Sci.* **2008**, *18*, 255–261. [[CrossRef](#)]
25. Dong, Y.; Du, J. Review on the typhoon effect on coastal aeolian land forms. *J. Desert Res.* **2014**, *34*, 634–638.
26. Yang, L.; Dong, Y.; Huang, D. Morphology and Grain Size of the Near Surface Sediment over Coastal Sand Sheet Response to Typhoon. *Sci. Geogr. Sin.* **2017**, *37*, 1243–1250.
27. Silva, F.G.; Wijnberg, K.M.; Hulscher, S. Storm-induced sediment supply to coastal dunes on sand flats. *Earth Surf. Dyn.* **2020**, *8*, 335–350. [[CrossRef](#)]
28. Sallenger, A.H., Jr. Storm impact scale for barrier islands. *J. Coast. Res.* **2000**, *16*, 890–895.
29. Jelgersma, S.M.; Stive, M.J.; Van der Valk, L. Holocene storm surge signatures in the coastal dunes of the western Netherlands. *Mar. Geol.* **1995**, *125*, 95–110. [[CrossRef](#)]
30. Cunningham, A.C.; Bakker, M.A.; Van Heteren, S.; Van Der Valk, B.; Van Der Spek, A.J.; Schaart, D.R.; Wallinga, J. Extracting storm-surge data from coastal dunes for improved assessment of flood risk. *Geology* **2011**, *39*, 1063–1066. [[CrossRef](#)]
31. Bateman, M.D.; Rushby, G.; Stein, S.; Ashurst, R.A.; Stevenson, D.; Jones, J.M.; Gehrels, W.R. Can sand dunes be used to study historic storm events? *Earth Surf. Process. Landf.* **2017**, *43*, 779–790. [[CrossRef](#)]
32. Dougherty, A.J. Prograded coastal barriers provide paleoenvironmental records of storms and sea level during late Quaternary highstands. *J. Quat. Sci.* **2018**, *33*, 501–517. [[CrossRef](#)]
33. Li, G.; Qi, F.; Nong, H.; Liao, S. Sedimentary facies sequences and evolutionary process of sedimentary environment of barrier-lagoons in Jiangping area, Guangxi. *J. Oceanogr. Huanghai Bohai Seas* **1999**, *17*, 8–18.
34. Li, C.; Chen, G.; Wang, P. The stratigraphic model of the Late- Quaternary barrier-lagoon depositional systems along the coast of China. *Acta Sedimentol. Sin.* **1991**, *9*, 12–19.
35. Chinese Gulf History Compilation Committee. *Chinese Gulf History (Volume 12, Gulf of Guangxi)*; China Ocean Press: Beijing, China, 1993; pp. 114–176.
36. Zhang, J. Division and Comparison of Quaternary Strata of Guangxi. *Guangxi Geol.* **1998**, *11*, 1–6.
37. Chen, B.; Qiu, S. Impacts of Typhoon Course and Landform on Water Level Fluctuation in the Coastal Bays in Guangxi. *Guangxi Sci.* **2000**, *7*, 282–285.

38. Reimer, P.J.; Bard, E.; Bayliss, A.; Beck, J.W.; Blackwell, P.G.; Ramsey, C.B.; Buck, C.E.; Cheng, H.; Edwards, R.L.; Friedrich, M.; et al. IntCal13 and Marine13 radiocarbon age calibration curves 0–50,000 years cal BP. *Radiocarbon* **2013**, *55*, 1869–1887. [[CrossRef](#)]
39. Duller GA, T.; Murray, A.S. Luminescence dating of sediments using individual mineral grains. *Geologos* **2000**, *5*, 87–106.
40. Mo, Y.; Liao, S.; Ge, W.; Li, P. Primary Analyses of the impacts to Guangxi Coastal Areas by modern sea level rise. *Guangxi Sci.* **1995**, *2*, 38–41.
41. Lu, H.; An, Z. Paleoclimatic significance of loess granularity compositions in Loess Plateau. *Chin. Sci. Bull.* **1997**, *42*, 66–69.
42. Si, Y.; Li, B.; Li, Z. A comparative analysis of grain size characteristics of modern aeolian sand and beach sand from the coast of Beibu Gulf in China. *J. Desert Res.* **2020**, *40*, 43–52.
43. Morton, R.A.; Gelfenbaum, G.; Jaffe, B.E. Physical criteria for distinguishing sandy tsunami and storm deposits using modern examples. *Sediment. Geol.* **2007**, *200*, 184–207. [[CrossRef](#)]
44. Folk, P.I.; Ward, W.C. Brazos Reviver bar: A study in the significance of grain size parameters. *J. Sediment. Petrol.* **1957**, *27*, 3–26. [[CrossRef](#)]
45. Chen, L.; Zhang, X. Mineral assemblages and their distribution pattern of the sediments from the Beibu Gulf. *Acta Oceanol. Sin.* **1986**, *8*, 340–346.
46. Li, P.; Ye, W. A study on heavy minerals of the surface deposits in the shallow area of Northern Beibu Gulf. *Trop. Oceanol.* **1987**, *6*, 39–47.
47. Kindle, M.E. Dominant factors in the formation of firm and soft sand beaches. *Sediment. Pet.* **1936**, *6*, 16–22.
48. Emery, K.O. Entrainment of air in beach sand. *J. Sediment. Petrol.* **1945**, *15*, 39–49. [[CrossRef](#)]
49. Frihy, O.E.; El Askary, M.A.; Deghidly, E.M.; Moufaddal, W.M. Distinguishing Fluvio-Marine Environments in the Nile Delta Using Heavy Minerals. *J. Coast. Res.* **1998**, *14*, 970–980.
50. Hubert, J.F. A zircon-tourmaline-rutile maturity index and the interdependence of the composition of heavy mineral assemblages with the gross composition and texture of sandstones. *J. Sediment. Res.* **1962**, *32*, 440–450.
51. Ren, Z.Y.; Zhao, X.; Liu, H. Dispersion Effects on Tsunami Propagation in South China Sea. *J. Earthq. Tsunami* **2015**, *9*. [[CrossRef](#)]
52. Yang, W.; Sun, L.; Yang, Z.; Gao, S.; Shao, D.; Mei, Y.; Zang, J.; Wang, Y.; Xie, Z. Nan' ao, an archaeological site of Song dynasty destroyed by tsunami. *Chin. Sci. Bull.* **2018**, *63*, 1–14.
53. Wen, K. *China Semeteorological Disasters Ceremony: Guangxi Volume*; Meteorological Press: Beijing, China, 2006.
54. Lv, M.; Ding, Y.; Shi, M. The response process of Typhoon China South Sea. *Trans. Oceanol. Limnol.* **2019**, *5*, 9–19.
55. Literature and History Research Museum of Tongzu Autonomous Region of Guangxi. *Natural Disaster Historical Materials of Guangxi*; The Second Library of Guangxi Zhuang Autonomous Region: Guangxi, China, 1978.
56. Dongling, L.; Hui, J.; Xiaoqun, X.; Longbin, S.; Tiegang, L. Freshwater diatoms in the Southern Okinawa trough and its implication to typhoon precipitation during the last millennium. *Quat. Sci.* **2015**, *35*, 755–766.
57. Oppo, D.W.; Rosenthal, Y.; Linsley, B.K. 2000-year-long temperature and hydrology reconstructions from the Indo-Pacific warm pool. *Nature* **2009**, *460*, 1113–1116. [[CrossRef](#)] [[PubMed](#)]
58. Moy, C.M.; Seltzer, G.O.; Rodbell, D.T.; Anderson, D.M. Variability of El Niño/Southern Oscillation activity at millennial timescales during the Holocene epoch. *Nature* **2002**, *420*, 162–165. [[CrossRef](#)] [[PubMed](#)]
59. Usoskin, I.G.; Solanki, S.K.; Kovaltsov, G.A. Grand minima and maxima of solar activity: New observational constraints. *Astron. Astrophys.* **2007**, *471*, 301–309. [[CrossRef](#)]
60. Yu, K.; Chen, T. Beach Sediments from Northern South China Sea Suggest High and Oscillating Sea Levels During the Late Holocene. *Earth Sci. Front.* **2009**, *16*, 138–145. [[CrossRef](#)]
61. Fang, G.; Li, P.; Huang, G. Sea level changes in Zhujiang Delta during the past 8000 years. *Geogr. Res.* **1991**, *10*, 1–11.
62. Li, X.; Li, X.; Zhao, Q.; Liu, L.; Zhou, S. The occurrence, acoustic characteristics, and significance of submerged reefs on the continental shelf edge and upper slope, northern South China Sea. *Cont. Shelf Res.* **2015**, *100*, 11–24. [[CrossRef](#)]
63. Gray, L.J.; Beer, M.; Geller, M.; Haigh, J.D.; Lockwood, M.; Matthes, K.; Cubasch, U.; Fleitmann, D.; Harrison, G.; Hood, L.; et al. Solar influence on Climate. *Rev. Geophys.* **2010**, *48*, 1032–1047. [[CrossRef](#)]